Carbon 227 (2024) 119211

Contents lists available at ScienceDirect

Carbon

journal homepage: www.elsevier.com/locate/carbon

Research paper

Multi-methodological analysis of hydrogen desorption from graphene

Francesco Delfino [a], Carles Ros [b], Sidney M. Palardonio [b], Nina M. Carretero [c], Sebastián Murcia-López [c], Juan Ramón Morante [c], Jordi Martorell [b,d], Zacharias G. Fthenakis [a], Mauro Francesco Sgroi [e,a], Valentina Tozzini [a,f], Luca Bellucci [a,*]

[a] Istituto Nanoscienze del Consiglio Nazionale delle Ricerche (CNR-NANO), NEST-SNS, Piazza San Silvestro, 12, Pisa, 56127, Italy
[b] ICFO, Institut de Ciencies Fotoniques, The Barcelona Institute of Science and Technology, Castelldefels, Spain
[c] IREC, Fundacion Instituto de Investigacion de la Energía de Cataluña, Jardins de les Dones de Negre 1, 2ª pl., Sant' Adrià del Besòs, Barcelona, 08930, Spain
[d] UPC, Departament de Física, Universitat Politecnica de Catalunya, Terrassa, 08222, Spain
[e] Department of Chemistry and NIS, University of Turin, Via Pietro Giuria 7, Torino, 10125, Italy
[f] INFN Sezione di Pisa, Largo Bruno Pontecorvo, Pisa, 56127, Italy

ARTICLE INFO

Keywords:
Graphene
Graphane
Hydrogen storage
Reactive molecular dynamics
Temperature-Programmed Desorption (TPD)

ABSTRACT

Chemisorption of hydrogen on graphene has been extensively investigated in last decades, but the reported values of over several eV, depending on different factors, such as the local structural environment, substrates or previously bound hydrogen.

In this work, we combine Temperature-Programmed Desorption experiments with simulations using empirical reactive force fields and Density Functional Theory calculations. We observe that desorption occurs through processes with different activation energies, which we are able to identify by analyzing simulation data and post-processing experimental ones through a procedure based on Arrhenius fit with feedback. The result is the assignment of experimentally observed desorption peaks to different desorption processes, namely desorption from isolated sp^3 H, or couples of H in conformation cis or trans, or edge sp^3 or sp^2 H.

The protocol we outline is generally applicable and might be particularly useful in more complex cases with larger multiplicity of desorption peaks.

1. Introduction

The chemisorption of hydrogen on graphene has been investigated since the very early days of graphene production, both experimentally [1,2] and theoretically [3]. In fact, graphene has been presented as an interesting material for stable, cheap, and safe mean for chemical hydrogen storage [4,5] and almost 1:1 H:C stoichiometry was recently demonstrated for hydrogenation of nanoporous graphene [6], possible when the structures allow accession to both faces of the graphenic surfaces. However, the process still presents some unclear aspects. In spite of the extensive experimental and theoretical investigation of graphene hydrogenation and dehydrogenation performed in the last decade, the values of binding and desorption energies present a certain variability in the literature, which is still a matter of debate. This study addresses the origin of this variability.

At the theoretical level, several *ab initio* calculations were aimed at evaluating the desorption/adsorption energy profile [7], which allows us to define the binding energies E_b as the differences in energies between bound and unbound states (see also Fig. 1)

$$E_b^{at} = E_{gr-H} - (E_{gr} + E_H) \qquad E_b^{mol} = E_{gr-H} - \left(E_{gr} + \frac{1}{2}E_{H_2}\right) \tag{1}$$

E_b^{at} and E_b^{mol} corresponding to the C–H binding energy with respect to atomic and molecular hydrogen, respectively, and E_{gr}, E_H, E_{H_2} and E_{gr-H} being the energies of graphene, atomic hydrogen, molecular hydrogen and hydrogenated graphene with a single H, respectively. By definition, E_b^{at} and E_b^{mol} are not independent, differing by the hydrogen molecule dissociation energy per atom $E_b^{H_2} = E_H - \frac{1}{2}E_{H_2} = E_b^{mol} - E_b^{at}$ whose value is known with a great accuracy [8]. Even restricting to Density Functional Theory (DFT) calculations, a large variety of values are found in the literature for E_a, E_b, and E_d, depending on the calculation setup and the pristine graphene conditions. In fact, graphene tends to bend after binding, therefore E_{gr-H} depends on the amount of relaxation allowed to the system, which in turn depends on the boundary conditions (isolated flakes and their size [9], periodic supercell and its tension [3,10]). The spin state of the graphene-hydrogen atom (gr-H) system also influences the binding energy [3], as well as the presence, distance, and conformation of other bounded atoms in the neighborhood of the chemisorbed H atom [7]. The overall hydrogen coverage and distribution influences E_b [11] destabilizing or stabilizing binding

* Corresponding author.
E-mail address: luca.bellucci@nano.cnr.it (L. Bellucci).

https://doi.org/10.1016/j.carbon.2024.119211
Received 1 March 2024; Received in revised form 22 April 2024; Accepted 2 May 2024
Available online 7 May 2024

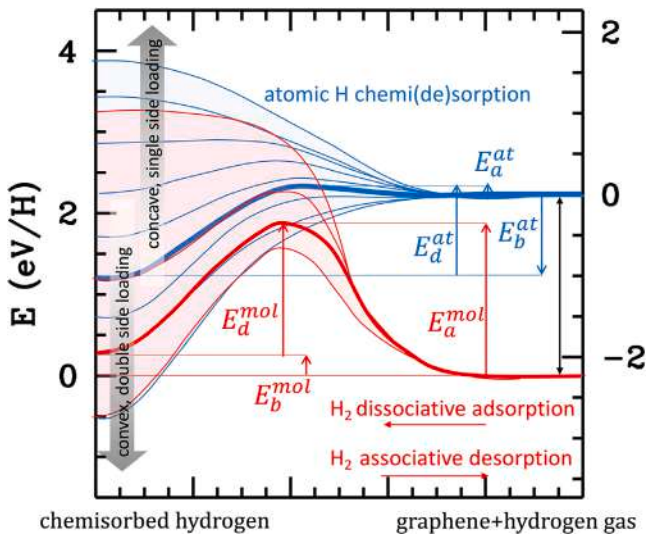

Fig. 1. Desorption/Adsorption energy profile for atomic H chemi(de)sorption on graphene. Blue lines (and shades) correspond to ad(de)sorption referred to atomic H, red lines (shades) to the process referred to the molecular hydrogen. Their difference is the H_2 binding energy, whose value is here taken as 2.23 eV [8]. Lines are qualitative drafts but reflect the real dependence on the curvature or coverage: thick lines are for pristinely flat graphene receiving an isolated H atom or a couple from a molecule, on nearby sites. The lines below are for pristinely convex, and/or previously double side loaded. Conversely above are for pristinely concave or pristinely single-side loaded sheets. (For interpretation of the references to color in this figure legend, the reader is referred to the web version of this article.)

in specific configurations such as 2 H atoms (dimers) in cis or trans conformations [3,7,12]. Convexities/concavities previously present on the sheet can influence binding up to 2.5 eV [13], and the different effects can combine theoretically leading to a variability of binding energies of several eV (shaded areas in Fig. 1). Calculations reveal the presence of energy barriers involved in adsorption/desorption, E_a and E_d (with $E_d - E_a = E_b$), also displaying a similar variability. In this case, the $E_{d/a}^{mol}$ and $E_{d/a}^{at}$ correspond to two different processes, that is the associative desorption/dissociative adsorption of H_2 and atomic chemi(de)sorption, respectively (in red and blue in Fig. 1), and therefore are not simply related. In the first process the molecule forms directly upon dissociation of two H atoms in nearby sites, or the other way round, the molecular dissociation occurs as the molecule binds to the sheet and the two H attach in nearby sites. For this process the activation energy E_a^{mol} is generally in the order of eV, required to dissociate the hydrogen molecule [14]. Combining graphene with transition metals capable of interfering with the molecular bond has been proposed to promote hydrogenation [15]. However, E_d^{mol} is reduced even in specific conditions, e.g. when H_2 desorption occurs between two H bound in nearby sites and concavities [13,16]. Conversely, for the adsorption of atomic hydrogen, only small barriers of a few tens of eV were reported [7,9], while desorption occurs with E_d of $\sim$ 1 eV, depending, as E_b the graphene condition and coverage. We report a non-exhaustive selection of energy values in the SI in Table S1, and a qualitative sketch of energy profiles in Fig. 1.

On the experimental side, several methods were used to study graphene hydrogenation. Clearly, adhesion of atomic H [1,2] is easier to achieve, due to its larger reactivity with respect to molecular form. Atomically resolved microscopy directly observed H preferential binding on convexities [14] often present in supported graphene, usually hydrogenated on a single side, although double side hydrogenation was achieved for suspended double side exposed graphene foams [1,2]. Besides direct observation, H binding can be measured through the change in electronic properties (typically, the band gap [1,14]), or by (spatially resolved) vibrational spectroscopy [17,18], or XPS spectra [19]. Although the shift in vibrational frequencies can give some indirect indications on the strength of binding, and XPS can measure to some extent the coverage, the method mainly used for evaluating the binding energy is the Temperature Programmed Desorption (TPD) [20]. TPD desorbs gases by increasing the temperature at a constant rate β, $T(t) = T_0 + \beta t$. The measured desorption rate of (molecular) hydrogen $R_{H_2}(t)$ is described by the Polanyi–Wigner (PW) equation [21]

$$R_{H_2}(T) = -\frac{1}{2}\frac{d\sigma_H}{dT} = \frac{1}{2}\frac{\nu_n}{\beta}\sigma_H^n e^{-\frac{E_d}{kT}} \quad (2)$$

from which one can evaluate E_d. The technique is quite robust and relatively cheap but depends on several parameters, such as the H-coverage σ_H, the order of the process n, and a pre-exponential factor ν_n, roughly representing the frequency of desorption attempts. These could be in principle fitted altogether on the measured temperature spectrum, potentially returning not only E_d, but also the σ_H and ν. In practice, however, the fitting procedure produces a large variability in the values. This was previously recognized and attributed to the sometimes arbitrary assumption on the value of ν and n [22].

In this work, we aim to determine the values of hydrogen binding and desorption energies from graphene samples. We adopt an unbiased procedure by combining fits with numerical iterative solutions of the PW equation. We apply the same procedure both to experimental data and to simulated TPD spectra using molecular dynamics with a Reactive Force Fields (ReaxFF) [23–25], which allow us to better analyze the different peaks arising in the experimental spectra. We finally compare the values obtained for the energies with the energy profiles from direct calculations using either the ReaxFF or DFT.

2. Methods

2.1. Samples and experimental analyses

Highly hydrogenated graphene was provided by Xlynx Materials Inc. (Victoria, Canada), in powder form, and analyzed with no further manipulation. The surface morphology was evaluated by field emission scanning electron microscopy (FEG-SEM, FEI Inspect F-EBL), revealing an exfoliated layered structure (Fig. 2(a)).

The samples were additionally analyzed before and after desorption by Raman and Fourier Transform Infrared (FTIR) spectroscopy measurements, acquired from powder samples placed in a crucible and annealed at different temperatures inside a tubular furnace in a 2 L/min flow N_2 atmosphere, previously purged for 1 h and ramped at 10 °C/min. FTIR spectra were recorded using a Cary 630 FTIR-ATR. The spectra were obtained after the compilation of 128 scans at 4 cm^{-1} resolution and are reported in Fig. 2(b). Raman spectra were obtained in a Renishaw inVia spectrometer, equipped with a 532 nm wavelength laser and 50x objective. To avoid sample damage or laser-induced reduction, the laser was attenuated to 0.05% power, 20 s exposition time, and 4 acquisitions (Figs. 2C and D).

Elemental analysis was performed with a TruSpec Micro CHNS analyzer from LECO. Data from X-ray diffractometry (XRD) was supplied by Xlynx Material Inc. (refer to Section S2 in the SI for additional information). Temperature-programmed Desorption (TPD) measurements were obtained using an AutoChem II 2920 V4.03 chemisorption analyzer coupled to a mass spectrometer (MS). Roughly 10 mg of highly hydrogenated graphene were used per experiment, and the temperature was raised from 30 °C to 900 °C at 10 °C/min under a constant 60 sccm/min constant Ar gas flow.

2.2. Density functional theory calculations

DFT spin resolved calculations were performed using the Perdew–Burke–Ernzerhof [26] (PBE) exchange and correlation functional with Grimme's D3 van der Waals corrections [27], a combination previously validated for graphene in interaction with hydrogen [28,29]. We used the supercells including 64 C atoms with periodic boundary conditions,

and the Projected Augmented Wave (PAW) approach combined with ultrasoft pseudopotentials as implemented in Quantum Espresso [30], with 65 Ry and 520 Ry cutoff for wavefunctions and density, respectively. Systems relaxations, either fully free or restraining the C–H distance around different values along the detachment path, were employed to evaluate the structure and energy of bound, and unbound states and barrier values of a hydrogen atom isolated or bound in dimers of different conformations, trans/cis and ortho, meta and para (six combinations).

2.3. Generation of hydrogenated graphene models

Classical Molecular Dynamics simulations were performed using LAMMPS [31] with the empirical CHON-2019 ReaxFF [24] proven reasonable in describing a variety of graphene-based materials and their interactions with C/H/N/O atoms [32,33]. To prepare hydrogenated graphene models, we followed a previously tested strategy [34] mimicking the experimental preparation procedure [35]. Graphene was simulated by a 264-atom supercell ($27 \times 25 Å^2$ large) periodically arranged along the xy plane. A separation of 40 Å between graphene sheets along the z direction was applied to ensure graphene isolation. Graphene was exposed to a reservoir of atomic H gas at two different temperatures, $T \sim 1250$ K or $T \sim 1400$ K and $P \sim 5000$ bar, under μVT conditions simulated by using the Grand Canonical Monte Carlo (GCMC) algorithm [36]. The chemical attack consisted of six GCMC of 2 ps each, during which exchanges of hydrogen atoms (insertion/deletion) took place every 2 ps. This procedure intentionally imposes extreme conditions, aiming to efficiently generate a series of random hydrogenated graphene models. Further 10 ps of standard MD simulation was performed to relax the systems. During relaxation, desorbed hydrogen was removed. From the procedure, six models were selected, with hydrogen coverage (σ_{cov}) evenly distributed from 41% to 78%, see Fig. S1 and S2 of SI, where a description of the models is reported.

2.4. Temperature programmed desorption simulations

The selected models were employed to generate two additional systems of double size, derived from the original one (see Fig. S1) by replicating along the x- or y-axis, respectively (see Fig. S3). Each set consisted of three systems, originating from the corresponding model at a fixed coverage. These systems were then subjected to TPD simulations to mimic the corresponding experiments: the system temperature increased step-wise from 300K to 3500K. The thermostat equations [37] were integrated with a timestep of 0.2 fs. At every 10 K interval, desorbed atoms were removed from the simulation. Two different temperature rates, denoted as β, were considered: 10^{11} °C/sec and 10^{12} °C/sec. The desorption curve presented for each coverage set represents the average outcome over three simulations, aiming to minimize statistical fluctuations (see Fig. S6 and Fig. S7). The cumulative simulation time for each model amounted to 100 ns, resulting in an overall total of 1800 ns.

2.5. Desorption curves analysis and Arrhenius fit

Both the TPD experiments and simulations generate TPD spectra, i.e. a rate curve $R_{H_2}(T)$ measuring the amount of desorbed hydrogen in each temperature interval. This is well described by PW Eq. (2), equivalently cast in the form of the Arrhenius plot

$$A(1/T) = \ln\left(\frac{R_{H_2}}{\sigma_H^n}\right) = -\frac{E_d}{kT} + \ln\left(\frac{\nu_n}{2\beta}\right) \tag{3}$$

obtained from the ratio of rate $R_{H_2}(T)$ and the residual coverage $\sigma_H(T)$ measured at the same T, evaluated as the ratio between the number of hydrogen atoms and carbon atoms (H/C) at the specific temperature. For a single process, and once the order of the process n is known $A(1/T)$ is a straight line, with slope $-E_d/k$ and intercept $ln(\nu_n/2\beta)$. While n is usually identified by attempt, we anticipate that our comparative analysis clearly identifies mostly 1st order processes, i.e. $n = 1$. For these, (corresponding in this case to detachment of atomic hydrogen) the Arrhenius plot is independent of the starting coverage, and the relation between the maximum of desorption spectrum T_p and the energy barrier E_d is

$$\frac{E_d}{kT_p} + \ln\left(\frac{E_d}{kT_p}\right) = \ln\left(\frac{\nu T_p}{\beta}\right) \tag{4}$$

which is an alternative way of evaluating E_d, provided ν is known. In the experimental practice it is customary to use the value $\nu = 10^{13}$ Hz, about one order of magnitude smaller than the related physical quantity, the C–H vibrational frequency, and to approximate the logarithmic addend in the first member with the empirical constant 3.4–3.5, which turns out a reasonable value if β is in the range of 0.1–0.2 °/s and the E_d in the range of 1–2 eV, and therefore $T_p \sim 400$–$700°$. While these combined approximations can lead to reasonable evaluation of the E_d in the experiment, the much larger β values of simulations do not allow us to use them. Therefore we proceeded to a fit with no *a priori* assumptions.

When different desorption processes are present, as is expected in this case, $R_{H_2}(T)$ is the convolution sum of single processes

$$R_{H_2}(T) = \frac{1}{2\beta}\sum_i \nu_i \sigma_i^{n_i} e^{-\frac{E_{d_i}}{kT}}, \tag{5}$$

where in principle all the parameters are process dependent. Clearly, the direct fit of such a large number of parameters may result poorly determined. Therefore the regression procedure was preconditioned using preliminary values obtained from a direct analysis of the Arrhenius plot: there, we identify the linearity intervals of T, where one of the single processes prevails, on which one fits the parameters of that process by linear regression. Those parameters are then used as starting values for the fit which is subsequently iteratively refined.

3. Results

Highly hydrogenated graphene samples observed by SEM present an exfoliated structure (Fig. 2(a)), with stacking of multiple graphene sheets forming 1-4 μm agglomerates. The thickness of the graphene layers cannot be resolved by SEM, but these are formed of 50 to 1000 nm highly corrugated domains characterized by a large number of edges, bending, and breakpoints.

3.1. Raman and FTIR spectra and elemental analysis

Data confirms the presence of C–H bonds with a main peak at 2850 cm^{-1}, proving that hydrogen is directly bonded to the graphene lattice. Up to the detection limit of this technique, no doublet peaks indicative of the presence of C–H_2 and C–H_3 groups are revealed [5]. Oxygen functional groups can be detected in 1000–1250 cm^{-1} region, and traces of nitrogen bonded to the substrate are detected at 3360 cm^{-1}. Upon annealing in N_2 atmosphere, the C–H bonds peak in FTIR is reduced at 400 °C and completely disappears for higher temperatures (Fig. 2(b)). X-ray diffractometry was performed on the material, revealing that the interlayer separation nearly doubled due to hydrogenation, consistent with previous findings [38]; see Section S2 and Fig. S4 in the SI.

The raw Raman spectra (Fig. 2(c)) is dominated by a significant fluoresce upon excitation with the 532 nm laser, due to the band gap opening caused by the significant presence of bonded hydrogen (see for instance Ref. [39]. After removing fluorescence as a baseline (Fig. 2(d)), the characteristic G peak for vibration of graphitic sp^2 domains (1582 cm^{-1}) is revealed to have a shoulder at 1594 cm^{-1}, which can be attributed to D' band of structurally-defective graphene. The D peak of defective graphene breathing mode (1350 cm^{-1}) is also

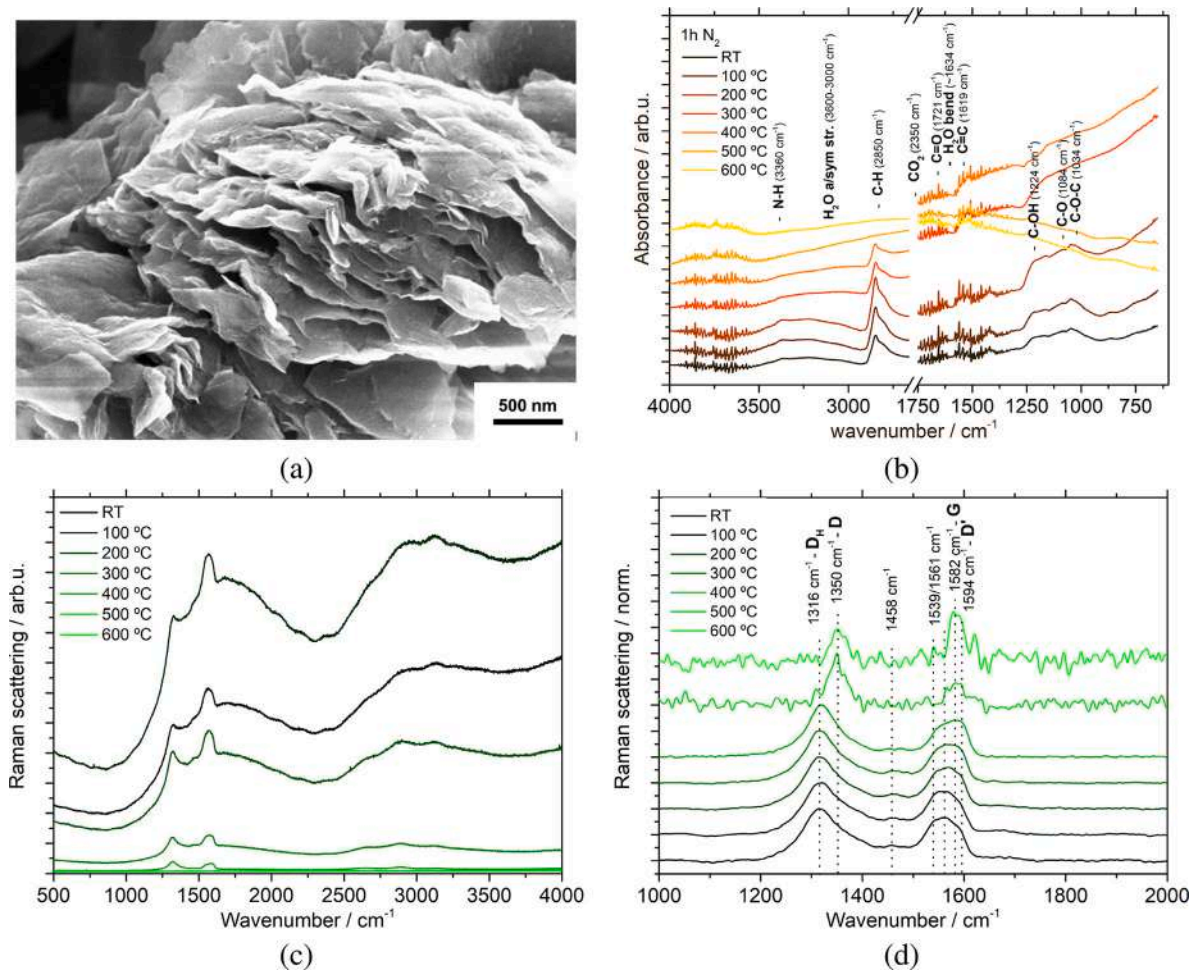

Fig. 2. (a) SEM image of a multiple stacking of highly hydrogenated graphene sheets in a highly hydrogenated graphene particle. (b) FTIR-ATR spectra of highly hydrogenated graphene powders from room temperature (RT) to annealed at 600 °C in a nitrogen atmosphere for 1 h. (c) Raman spectra acquired with excitation with the 532 nm laser at different temperatures. (d) The same data after baseline subtraction and normalization to the G peak.

revealed, with a stronger neighbor peak at 1316 cm^{-1} here named D_H. Usually, the positions, intensity, and width of defect-associated bands (D and D') arise due to the presence of ruptures in the crystal lattice of graphene [40]. Poorly understood shoulder peaks at 1539/1561 cm^{-1} and an inter-band at 1458 cm^{-1} are also present. It must be noted that the untreated sample (labeled as RT, room temperature) has a lower signal for both FTIR and Raman fluorescence compared with the one annealed at 100 °C, which can be caused by the presence of ambient humidity physisorbed on the surface of the material (see SI section S3 and Fig. S5) affecting local atomic conformation. Raman spectroscopy shows a major loss of fluorescence at > 100 °C (Fig. 2(c)), gradually decreasing with increased temperature. At 300 °C the oxygen and nitrogen functional groups are observed to disappear from the FTIR peaks, correlating with TPD-MS measurements (Fig. S5). For annealing processes starting at 400 °C, a complete removal of the C–H bonds is observed by FTIR. At higher than 400 °C treatments the characteristic defective graphene structure is recovered, reducing the C–C bond length, and presenting a narrower G peak and a smaller D peak, which are clearly blueshifted compared with the D_H peak, all suggesting the reestablishment of order in the lattice. Thus, Raman and FTIR-ATR spectroscopies can detect variations in the high hydrogen-containing samples due to variations in photo-luminescence at low binding energies (temperature treatments), and the loss of the major part of H, with stronger bonding, at higher temperatures. The poorly understood shoulder peaks at 1539/1561 cm^{-1} and an inter-band at 1458 cm^{-1} seem to be associated only with hydrogenated samples and point to the relationship of the disappearance of H binding with hydrogen removal.

3.2. Experimental TPD curves

In this section, we report and discuss the set of desorption energies as extracted from TPD experiments and simulations, following the procedure described in Sections 2.5 and 2.4, and compare them to direct calculations of the desorption energy barriers. The TPD measurements of hydrogenated graphene are reported in the SI (sections S3). Elemental analyses of the pristine sample agree on values of the H loading of 4.2% in mass, corresponding to the stoichiometry $C_1H_{0.53}$, i.e. 53% of coverage.

Although samples include traces of other elements, here we focus on the desorption spectra of hydrogen, shown in Fig. 3(a). The profile displays multiple peaks in the range 400–1200 K, with a main one at ~800 K, indicating several non-equivalent C–H bonds. The Arrhenius plot is shown in Fig. 3(b)) and identified three linear intervals, that we used to extract preliminary information on the dominant processes in those regions via the linear regression. Considering that the parameter ν is physically related to the vibrational frequency of the C–H modes and that this is known to vary by < 10% (Fig. 2(b)), and that it contributes logarithmically to the intercept, it is reasonable to consider a single ν value for all the components. The values of ν and E_d are reported in Table 1. We then perform the convolution fit with the function (5) including five first-order processes with the same ν, using the

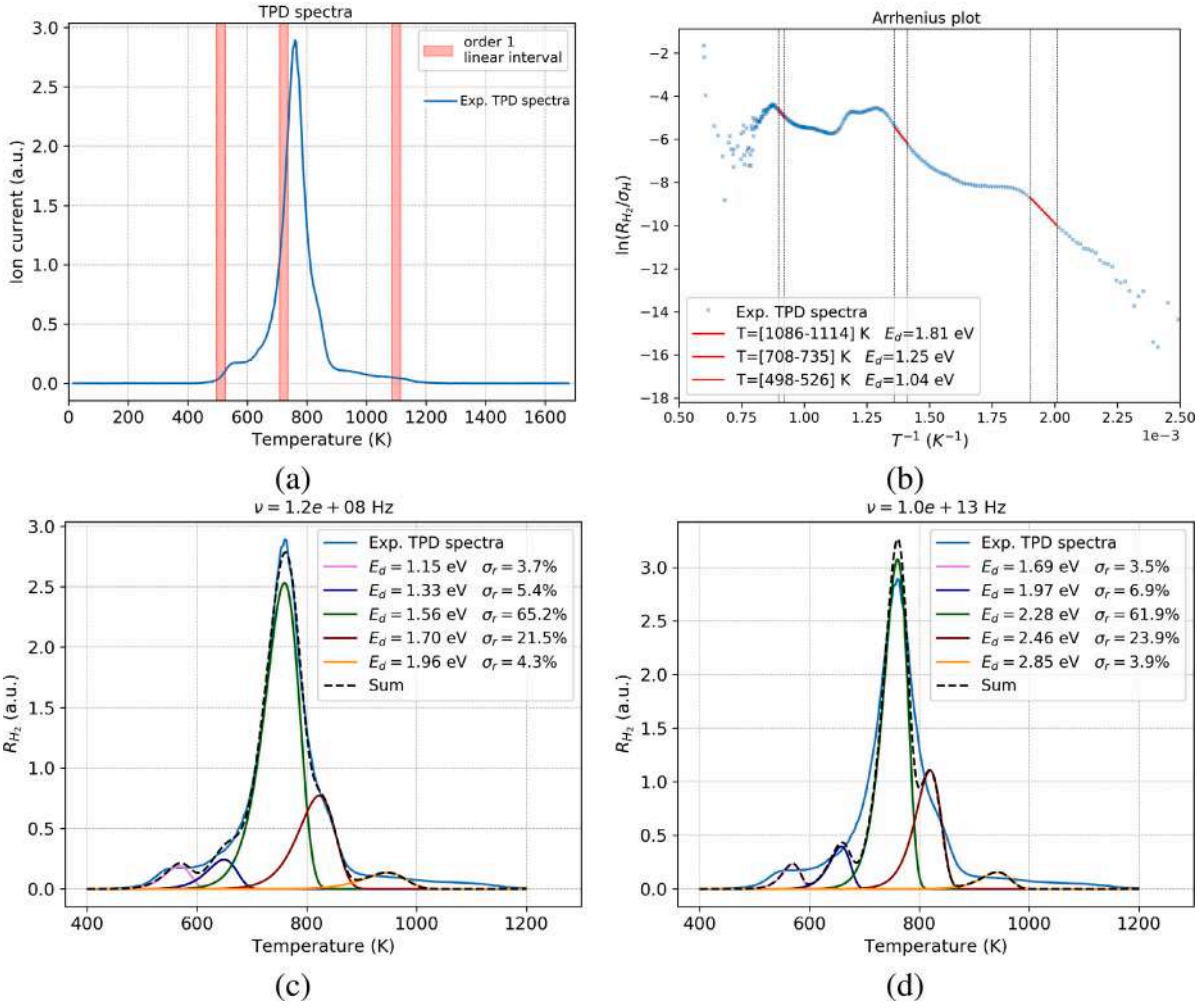

Fig. 3. (a) Experimental mass spectroscopy measurements of curves of hydrogen desorption from graphene during TPD experiments (see also section S3 and Fig. S5 for more details). Highlighted in red are the intervals of linearity in the Arrhenius plot (b). (b) Arrhenius plot with $n = 1$ of the desorption profile (a). Red lines correspond to linear regressions in the selected intervals. (c) Convolution fitting of the desorption profile with the fitted value of ν. The fitted values of the desorption energy (E_d) and the relative coverages defined as $\sigma_r = (\frac{\sigma_H(T)}{\sigma_{cov}}\%)$ are indicated in the visual legend. Different colors correspond to component desorption processes. (d) Same as (c), with a fixed value of $\nu = 10^{13}$ Hz. (For interpretation of the references to color in this figure legend, the reader is referred to the web version of this article.)

parameters obtained from the linear fit as starting values. The results are shown in Fig. 3 and reported in Table 1. The fit can resolve the five peaks giving values of E_d slightly larger than the starting one and returning a total convolution curve that superimposes very well on the experimental data (black dashed vs blue line in Fig. 3(c)). The relative amounts of the different components are also resolved, indicating the most abundant, the peak named "sp^3". The fit of experimental data cannot give an assignment to specific processes, which is conversely possible with the simulation data and discussed later on in Section 3.3, after which the names were assigned to the five TPD peaks.

The fitted value of the frequency is $\sim 10^8$ Hz, larger than the starting value but still quite lower than C–H vibrational frequencies. We then repeated the fit fixing to the value $\nu_1 = 10^{13}$ Hz, the empirical value, and $\nu_2 = 1.3 \times 10^{14}$ Hz, i.e. the typical frequency of the C–H modes. These larger values of ν produce sharper peaks (see Fig. 3(d)), which decrease overall the quality of the fit. In turn, larger values of ν produce systematically larger values of the E_d. Interestingly, the values obtained with $\nu_1 = 10^{13}$ Hz are those best matching the theoretical direct calculations of barriers, as shown in the next sections. This apparent discrepancy between the value of ν that best fits the peak width and that gives the best match with the energies but narrower peaks, could be explained by the presence of other sources of errors contributing to the width of the peaks in the experiment, aside the C–H fluctuations.

3.3. Simulated TPD curves and comparison

The analysis and fitting procedure repeated on the simulated TPD data allows us to assign the peaks to specific desorption processes. The desorption profiles at different starting coverage and with the two simulated temperature rates $\beta = 10^{11}$ and 10^{12} K/s are reported in Fig. 4. Clearly, due to the extremely different value of β used in simulations, the T_p position is moved to higher temperatures, in the range 2000–2500 K. Up to $\sigma_{cov} = 65.5\%$ of, we do not observe any dependence of the peaks shape and position on the starting coverage, while for the two largest coverages ($\sigma_{cov} = 76.1, 78.4\%$) we observe the appearance of new peaks in the high energy regions, indicating the activation of new processes. Among these, ruptures of the sheet and detachment of larger carbon moieties were also observed, which are not likely to be present in the experiment conducted at much lower temperatures. The substantial independence of the peaks from the coverage justifies the use of single-order formulas for the experimental data, where coverage is less than or around 50%, and for the lower coverage simulation data, while more attention is required for the high coverage simulations, although even in these cases the first order direct desorption appears prevalent over the associative desorption, from the direct analysis of simulation trajectories.

Simulations give access to the analysis of the single components of the total desorption profile, by post-processing the trajectories and

Table 1
Desorption barriers (E_d), frequency factors (ν), starting relative surface H coverage σ_r of different C–H desorption processes extracted with the different methods from simulations (sim) and experimental (exp) TPD curves. The peaks are named by their prevalent component. "sp^3" is a superposition of basically all internal sp^3 type sites, although the most populated are those in trans conformation (see Fig. S2).

	Method	data	β (K/s)	C–H type	E_d (eV)	ν (s^{-1})	σ_r (%)
A	direct fit	exp	0.16		1.04	1.9×10^6	
	direct fit	exp	0.16		1.25	1.9×10^6	
	direct fit	exp	0.16		1.81	1.9×10^6	
B	conv fit, unrestrained ν	exp	0.16	sp^3 iso	1.15	1.2×10^8	3.7
	conv fit, unrestrained ν	exp	0.16	sp^3 cis/iso	1.33	1.2×10^8	5.4
	conv fit, unrestrained ν	exp	0.16	sp^3	1.56	1.2×10^8	65.2
	conv fit, unrestrained ν	exp	0.16	edge sp^3	1.70	1.2×10^8	21.5
	conv fit, unrestrained ν	exp	0.16	edge sp^2	1.96	1.2×10^8	4.3
C	conv fit, fixed ν_1	exp	0.16	sp^3 iso	1.69	1.0×10^{13}	3.5
	conv fit, fixed ν_1	exp	0.16	sp^3 cis/iso	1.97	1.0×10^{13}	6.9
	conv fit, fixed ν_1	exp	0.16	sp^3	2.28	1.0×10^{13}	61.9
	conv fit, fixed ν_1	exp	0.16	edge sp^3	2.46	1.0×10^{13}	23.9
	conv fit, fixed ν_1	exp	0.16	edge sp^2	2.85	1.0×10^{13}	3.9
D	conv fit, fixed ν_2	exp	0.16	sp^3 iso	1.81	1.3×10^{14}	3.4
	conv fit, fixed ν_2	exp	0.16	sp^3 cis/iso	2.10	1.3×10^{14}	6.8
	conv fit, fixed ν_2	exp	0.16	sp^3	2.44	1.3×10^{14}	61.4
	conv fit, fixed ν_2	exp	0.16	edge sp^3	2.63	1.3×10^{14}	24.6
	conv fit, fixed ν_2	exp	0.16	edge sp^2	3.05	1.3×10^{14}	3.8
E	convolution fit	sim	10^{11}	sp^3 cis/iso	1.92 ± 0.11	1.3×10^{14}	1.9 ± 0.1
	convolution fit	sim	10^{11}	sp^3	2.26 ± 0.01	1.3×10^{14}	55.0 ± 4.1
	convolution fit	sim	10^{11}	edge sp^3	2.43 ± 0.10	1.3×10^{14}	32.2 ± 3.8
	convolution fit	sim	10^{11}	edge sp^2	2.97 ± 0.04	1.3×10^{14}	10.9 ± 1.4
F	convolution fit	sim	10^{12}	sp^3 cis/iso	2.04 ± 0.05	1.3×10^{14}	1.8 ± 0.1
	convolution fit	sim	10^{12}	sp^3	2.26 ± 0.02	1.3×10^{14}	56.5 ± 5.8
	convolution fit	sim	10^{12}	edge sp^3	2.40 ± 0.06	1.3×10^{14}	27.6 ± 1.8
	convolution fit	sim	10^{12}	edge sp^2	2.86 ± 0.03	1.3×10^{14}	14.1 ± 5.5
G	direct fit	sim		sp^3 cis/iso	2.06 ± 0.14	1.3×10^{14}	1.0
	direct fit	sim		sp^3	2.17 ± 0.13	1.3×10^{14}	48.1
	direct fit	sim		edge sp^3	2.50 ± 0.09	1.3×10^{14}	43.1
	direct fit	sim		edge sp^2	2.95 ± 0.12	1.3×10^{14}	7.8

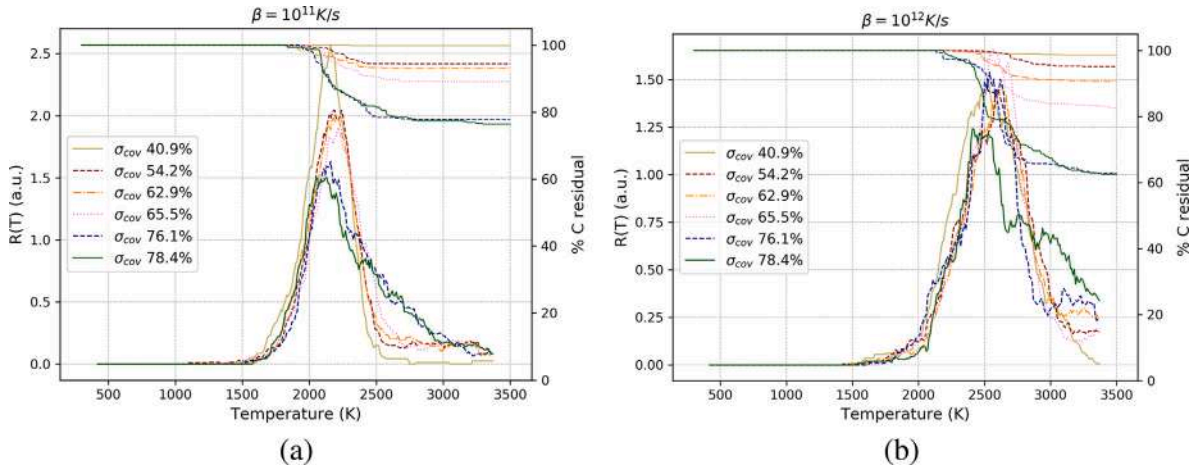

Fig. 4. Simulation TPD curves of hydrogen desorption from graphene at different starting σ_{cov}, at the two different simulated heating rates $\beta = 10^{11} K/s$ (a) and $\beta = 10^{12} K/s$ (b). The bell-shaped lines are the desorption rates with scales on the left, The upper lines report the residual C on the sheet, with the scale read on the right.

selecting desorption process types. In Figs. 5 (a) and 5 (b), we report in different colors the desorption profiles corresponding to desorption from given C–H bond types, in the simulations with the two values of β (indicated) and for a selected initial hydrogen coverage of 62.9% (profiles for the other starting coverages are reported in the SI, section S4). The analysis allows unambiguously assigning the higher temperature peaks to desorption from edges, in sp^2 or sp^3 conformation (orange and red curves in Fig. 5). The desorption from internal sites, conversely, is more difficult to resolve. We classify the type of sites in isolated, or dimers in cis (same side of the sheet) or trans (opposite side, see Fig. 5 and legends for the color coding). The analysis indicates that the peaks corresponding to these three types are partially superimposed, although isolated and cis dimer conformation appears to contribute to the lower temperatures. Based on these observations, we assigned the experimental peaks as summarized in Table 1. Interestingly, the edges, initially absent in simulations, form during heating, producing a population of edge-bonded atoms and their subsequent desorption. This is the origin of the "negative" anomaly in the desorption profile for edge hydrogen (red and yellow curves).

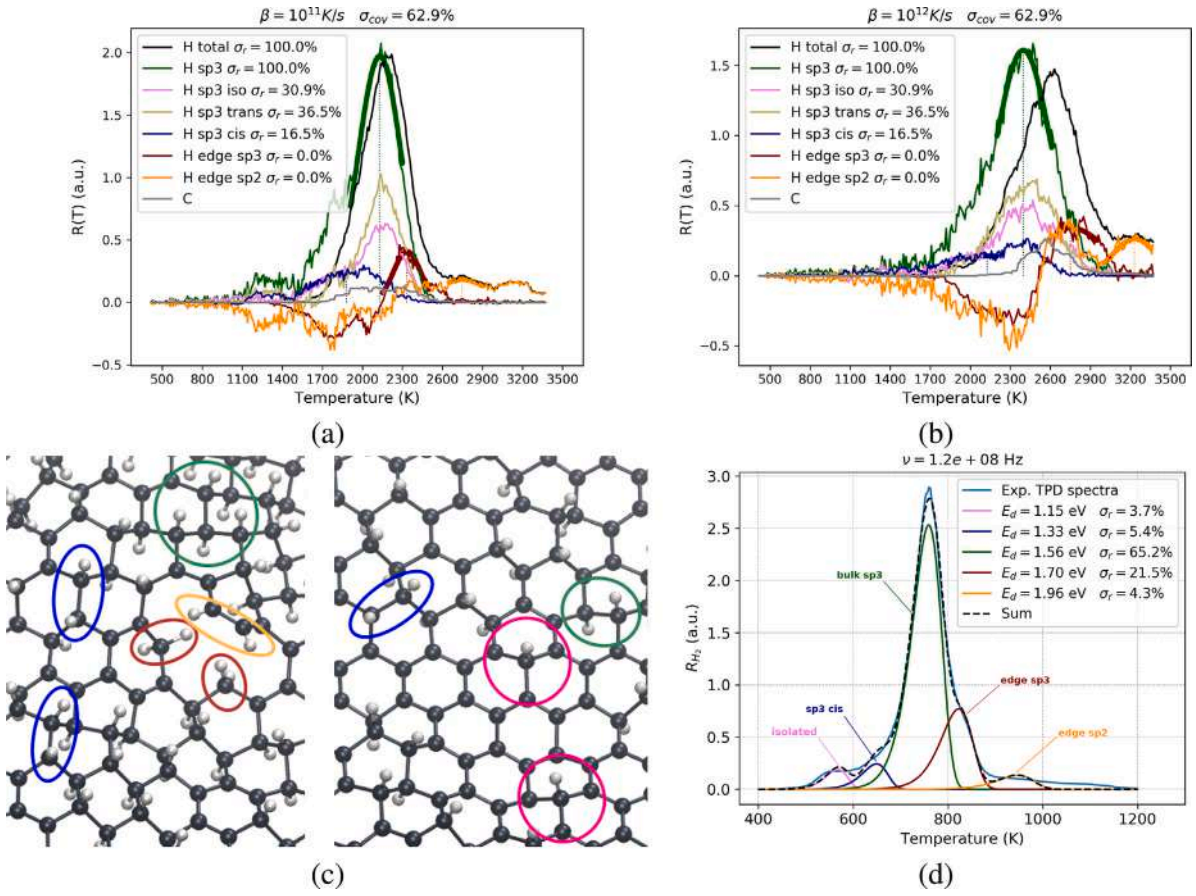

Fig. 5. (a, b) Desorption profiles of different C–H configurations, for $\beta = 10^{11} K/s$ and $10^{12} K/s$, respectively. The color legend is the following: black, total desorption profile of hydrogen atoms; green, bulk sp^3 C–H bonds, usually in trans conformation (light green); pink, isolated bulk sp^3 C–H bonds; blue, pairs of C–H bonds in cis conformation; red, edge sp^3 C–H bonds; orange edge sp^2 C–H bonds; gray, desorption profile of carbon atoms. (c) Visual representation of the above-mentioned C–H configurations encircled with the corresponding color. (c) Association of the experimental convolution fit peaks with the above-identified peaks in simulations. (For interpretation of the references to color in this figure legend, the reader is referred to the web version of this article.)

The experimental peaks are assigned by analogy (Fig. 5(d)). Starting from the highest energy, the assignment of edge sp^2 peak (yellow) is unambiguous, and the separation of edge sp^3 peak (red) clear enough (see also Fig. 6, same color coding); also quite clear, though in part mixed with the central sp^3 peak (green) are the peaks associated to the cis desorption (blue) and to the isolated one (pink) that in the experiment appear better resolved than in the simulation. We will discuss this point more in detail in the next section.

As for the experimental ones, we analyzed the simulation TPD curves with the convolution fit. Since, as observed, the low energy peaks are very weak in this case, the fit is performed using Eq. (5) of four processes only. In this case, we used the theoretical value of $\nu = 1.3 \times 10^{14}$ Hz, which however turns out to better fit the relatively narrower peaks. This is consistent with the fact that in simulation the vibrational motion and dynamic of the system is the only source of the peaks enlargement. The values of E_d extracted from the convolution fit are plotted as a function of the starting H coverage in Fig. S9 (see also SI, section S4), and show little dependence on it, as already noted. Their averages are reported in Table 1.

The E_b value can be estimated also fitting directly the peaks position with Eq. (4), taking advantage of the fact that each single process can be separated, and that for each we have two different determinations with two different β values. Using Gaussian shapes for the peaks, we estimate $T_p(\beta)$ for the separate processes and coverages. Coherently with the previous strategies, we fitted a single frequency value, returning 1.3×10^{14} Hz, which roughly corresponds to the average C–H vibrational frequency. The values of E_d extracted by the direct fit are reported in the SI in Fig. S9(c) as a function of the coverage, showing again little dependence, while the average values are reported in Table 1.

3.4. Direct calculations of barriers and discussion

To resolve the remaining ambiguities of assignment we now include into the discussion the direct calculations of E_d, E_b, and E_a from DFT or ReaxFF, reported in Table 2. Because the edge desorption peaks are already unambiguously assigned, we performed only calculations for sp^3 internal atoms and in the most likely configurations, that is, the isolated H on the sheet or "dimers", i.e. nearby adsorbed atoms in the configurations ortho meta and para and from the same side of the sheet (cis) or opposite side (trans). In all cases the desorption is of single atoms, leaving the other one on the sheet. Looking first at the ReaxFF desorption energies, we observe that the values of E_d for the isolated, ortho and para conformations are similar with those obtained from the main peak of the simulated TPD and confirm the assignment of this peak to a mixture of the more stable conformation of internal H atoms. As noted, E_d for the isolated atom superimposes in energy to the ortho-cis and with the para values, while the ortho-trans appears at slightly larger energies. Conversely, the E_d values of the meta energies are substantially lower, but do not contribute to the TPD simulations because meta conformations are considerably less stable and therefore little populated, giving low statistical contribution to the TPD curve.

The DFT E_d values are correlated with the Reax ones, although 10%–15% smaller (see Fig. 6, red vs green dots). The difference can be explained by the fact that ReaxFF is generally optimized to reproduce the different chemical state, but are known to be less accurate on the transition states especially when it involves radicals or complex spin states. Accordingly, we observe the larger discrepancies in the isolated and meta cases, which among all are those where the graphene

Table 2
Binding and barrier energies as defined in Fig. 1. In each case, the considered process is the extraction of a single atom, from the configurations indicated in the second column. The unbound state is the detached atom at ~ 10 Å from the graphene sheet. Energies are per H atom.

	System	E_b (eV)	E_a (eV)	E_d (eV)
DFT	isolated	−1.3	0.3	1.6
	dim ortho cis	−1.79	0.7	2.5
	dim ortho trans	−2.36	0.19	2.55
	dim meta cis	−0.65	0.27	0.92
	dim meta trans	−0.60	0.29	0.89
	dim para cis	−1.75	0.32	2.07
	dim para trans	−1.57	0.36	1.93
Reax	isolated	−1.37	0.88	2.25
	dim ortho cis	−1.61	0.63	2.24
	dim ortho trans	−2.19	0.48	2.67
	dim meta cis	−1.15	0.51	1.66
	dim meta trans	−1.14	0.53	1.67
	dim para cis	−1.62	0.74	2.36
	dim para trans	−1.4	0.79	2.19

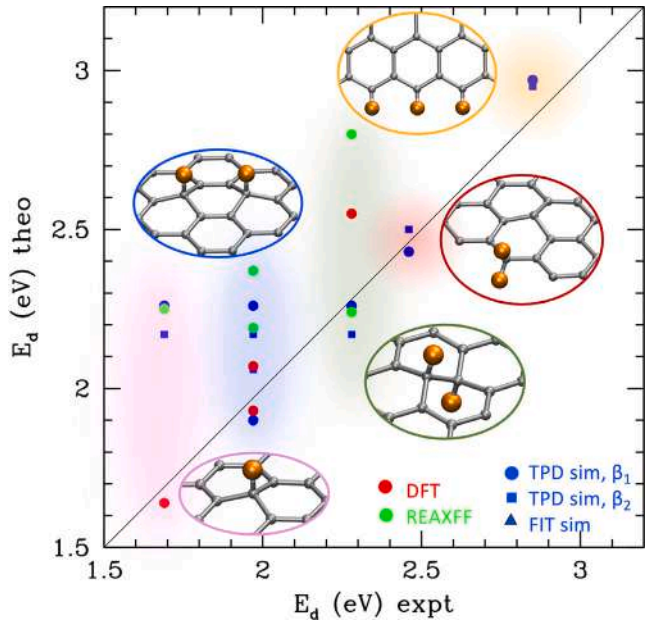

Fig. 6. Correlation plot of theoretical determinations of E_d vs experimental ones. The set of experimental data determined with the convolution fit and frequency ν_1 (see Table 1, set C) is used as the reference, and theoretical determinations (Reax TPD sim in blue, circles = set D, squares = set F, triangles = set G, ReaxFF direct calculations in green and DFT calculations in red, as per visual legend) are plotted vs it. Data are grouped with shaded areas colored according to the different types of sites, with the same colors as in previous Figs, and representative structures for each group are reported in the ovals, contoured with the same colors. (For interpretation of the references to color in this figure legend, the reader is referred to the web version of this article.)

sheet is magnetically polarized (see the SI, section S5). However, meta-dimers do not affect this discussion, since as previously observed, their stability and population are very small. The case of isolated H atoms, conversely, deserves a discussion. DFT calculations return an E_d value for the isolated H (~ 1.6 eV) compatible with the low energy peak observed experimentally. Our calculations reveal that this value has a large variability, which is consistent with the values reported in the literature. The reason is that the stability of isolated internal H is particularly sensitive to the local curvature of the sheet [13], see also the SI, section S6, with values of ~ 1 eV on completely flat graphene, increasing up to > 2 eV when the sheet corrugates. In the table we reported an average value that is likely to be more consistent with the real situation where thermal ripples are present. The problem is not present in the dimers, where the main factor affecting the E_d is the vicinity and conformation (ortho/meta/para, cis/trans) of the second atom. Additionally, although the population of isolated H is not large in the observed simulations, isolated H are indeed present, especially at lower coverages, since they are more stable than meta dimers. This allows us to hypothesize the assignment of the low energy elusive experimental peak to the isolated H atom (see pink shaded area in Fig. 6).

The ortho cis-dimer deserves a separate discussion. ReaxFF predicts for this case a barrier lower than for the trans one, while, conversely, DFT predict a high barrier. It must be noted however, that the transition state in this case is very elusive because the process is competitive with the associative desorption, in which the H is captured by the other one in the nearby site and together are desorbed as H_2 (this process turns out negligible in all other cases, either because the atoms are too far or because on different sides of the sheet). This causes a very large error in the determination of E_d in this case. While this is the only case in which the first order analysis might not be applied, we also observe that in the dynamical simulations (and in real experiment) the phase space offered to single H for escaping to the other H capture is larger, and therefore the second order process definitely suppressed.

Fig. 6 finally reports a summary of the E_d values calculated with various methods and plotted against those extracted from the experimental convolution fit with ν_1 (set C in Table 1), which we consider the most reliable set of experimental data, and our hypothesized peaks assignment. Blue dots are the data extracted from fits of the TPD simulation, red and green are the direct calculations of E_d either from DFT or ReaxFF. Edge-sp^2 and edge-sp^3 (red and yellow shades and contours, respectively) show a good correlation with experimental data, and therefore a clear assignment. We consider also quite clear the assignment of the isolated conformation (pink shade and contour), although in this case only the DFT datum (red dot) matches numerically with the experiment, for the reason previously discussed. Less clear is the precise assignment of the intermediate region peaks, given the larger spread of energies and superposition of peaks. However, the larger stability and population of trans (especially ortho-trans) configurations suggest the assignment of the main peaks to these (green shaded area and green contoured ovals), while the secondary peak seems mainly associatable to the less stable cis conformations (blue shaded areas). We reported the para one, best matching the energy value, but we do not exclude the presence of ortho cis, whose desorption, however, may also occur through a second order process in alternative to the first order one.

4. Summary and conclusions

In conclusion, in this work we have reported an extensive study of TPD from highly hydrogenated graphene combining experimental data, molecular dynamics simulations and advanced fits analyses with Arrhenius plots and Polanyi–Wigner approach. The initial convolution fit on experimental data returned a multi-first-order process picture, with at least five distinct desorption energies E_d. We obtained different sets of values for E_d corresponding to different values of the frequency pre-factor ν, a parameter that should be physically related to the vibrational frequency of C–H modes, but that in fact, is conventionally set at smaller values. From direct fit, we find a that a value appropriate to fit the TPD peaks width would be very small (i.e. 7–8 orders of magnitude smaller than the actual C–H frequency), and in turn produce too small values of the desorption energies. Conversely, values near to the actual physical value of C–H frequency 10^{14} Hz or 10^{13} Hz, a value often used in the literature, produce reasonable values of the E_b but narrower peaks than the experimental ones. This is attributed to the presence of additional sources of experimental peak enlargement aside from the C–H vibrations.

The same procedures applied to the TPD simulations can take advantage of the possibility of separating the single processes explicitly by the post-processing of the simulation trajectory. In addition, simulations include no source of peak enlargement other than the vibrations and dynamics of the system.

This brings two main results: (i) we were able to assign the peaks to specific processes, corresponding to edge sp^2 and sp^3 desorption and to internal H desorption, in turn classified in isolated cis or trans, though with large superpositions, and to transpose this assignment in the experimental peaks, and (ii) we were also able to verify that the high value of ν corresponding to the physical C–H frequency, in the simulation data, gives a good fit of the TPD curve, and is therefore consistent with the whole picture. In order to better resolve the main peaks associate to the desorption of H in sp^3 conformation from the internal H atoms, we compared the fitted E_d data with those obtained from direct calculations of the desorption energy profile, either by DFT and ReaxFF. With Reax, we obtain values coherent with the TPD Reax simulations, which allow us to further analyze the peak in sp^3 from ortho, meta and para conformations. The assignment of the low energy peak observed in experiment remains still elusive, since this is not resolved in ReaxFF simulations. However DFT calculations indicate that its energy is compatible with that of isolated H desorption, not visible in ReaxFF. The comparative analysis of DFT and ReaxFF data with simulation allow to give hypotheses to resolve the assignment of the superimposed peaks, the main one resulting prevalently in ortho-trans conformation, while the smaller one including a mixture of the other cases (with the possible exception of the very weakly populated meta states).

This combined technique allows to give an accurate representation of the processes occurring during TPD and the complete assignment of the desorption peaks observed in experiment. This procedure is proven effective and accurate, and is particularly useful in cases when the multiplicity of processes is high.

CRediT authorship contribution statement

Francesco Delfino: Data curation. **Carles Ros:** Writing – review & editing, Methodology, Investigation, Data curation, Conceptualization. **Sidney M. Palardonio:** Data curation. **Nina M. Carretero:** Data curation. **Sebastián Murcia-López:** Data curation. **Juan Ramón Morante:** Data curation. **Jordi Martorell:** Supervision, Funding acquisition, Conceptualization. **Zacharias G. Fthenakis:** Writing – review & editing, Methodology. **Mauro Francesco Sgroi:** Writing – review & editing, Conceptualization. **Valentina Tozzini:** Writing – review & editing, Writing – original draft, Funding acquisition, Formal analysis, Data curation, Conceptualization. **Luca Bellucci:** Writing – review & editing, Writing – original draft, Visualization, Supervision, Funding acquisition, Software, Methodology, Investigation, Conceptualization.

Declaration of competing interest

The authors declare the following financial interests/personal relationships which may be considered as potential competing interests: Luca Bellucci reports financial support was provided by European Union's Horizon 2020. If there are other authors, they declare that they have no known competing financial interests or personal relationships that could have appeared to influence the work reported in this paper.

Acknowledgments

This research was supported by EU under FETPROACT LESGO (Agreement No. 952068) and by the Italian University and Research Ministry, Ministero dell'Istruzione, dell'Università e della Ricerca under MONSTRE-2D PRIN2017 KFMJ8E and under the PNRR Mission 4 - Component 2 - Investment 1.1 "Fondo per il Programma Nazionale di Ricerca e Progetti di Rilevante Interesse Nazionale (PRIN)" funded by the European Union - Next Generation EU, project PRIN2022-202278NHAM (PE11) CHERICH-C "Chemical and electrochemical energy storage materials from organic wastes: the treasure hidden in C based materials". We acknowledge the allocation of computer resources from CINECA, through the ISCRA B projects IsB27_SETE (no. HP10BSTFDD), and IsC94_LESGO (no. HP10CEFAH5). ICFO additionally acknowledge financial support from CEX2019-000910-S (MCIN/AEI/10.13039/501100011033), BIST, Fundació Cellex, Fundació Mir-Puig, and Generalitat de Catalunya through CERCA. C.R. acknowledges support from the MCIN/AEI (FJC2020-043223-I) and the Severo Ochoa Excellence Post-doctoral Fellowship (CEX2019-000910-S). S.P. acknowledges support from the Generalitat de Catalunya - Joan Oró Fellowships (2023 FI-2 00390).

Appendix A. Supplementary data

Supplementary material related to this article can be found online at https://doi.org/10.1016/j.carbon.2024.119211.

References

[1] D.C. Elias, R.R. Nair, T.M.G. Mohiuddin, S.V. Morozov, P. Blake, M.P. Halsall, A.C. Ferrari, D.W. Boukhvalov, M.I. Katsnelson, A.K. Geim, K.S. Novoselov, Control of graphene's properties by reversible hydrogenation: Evidence for graphane, Science 323 (5914) (2009) 610–613, http://dx.doi.org/10.1126/science.1167130.

[2] M.M.S. Abdelnabi, E. Blundo, M.G. Betti, G. Cavoto, E. Placidi, A. Polimeni, A. Ruocco, K. Hu, Y. Ito, C. Mariani, Towards free-standing graphane: atomic hydrogen and deuterium bonding to nano-porous graphene, Nanotechnology 32 (3) (2020) 035707, http://dx.doi.org/10.1088/1361-6528/abbe56.

[3] D.W. Boukhvalov, M.I. Katsnelson, A.I. Lichtenstein, Hydrogen on graphene: Electronic structure, total energy, structural distortions and magnetism from first-principles calculations, Phys. Rev. B 77 (2008) 035427, http://dx.doi.org/10.1103/PhysRevB.77.035427.

[4] L. Ciammaruchi, L. Bellucci, G.C. Castillo, G.M.-D. Sánchez, Q. Liu, V. Tozzini, J. Martorell, Water splitting of hydrogen chemisorbed in graphene oxide dynamically evolves into a graphane lattice, Carbon 153 (2019) 234–241, http://dx.doi.org/10.1016/j.carbon.2019.06.087.

[5] A. Pinilla-Sánchez, E. Chávez-Angel, S. Murcia-López, N.M. Carretero, S.M. Palardonio, P. Xiao, D. Rueda-García, C.M. Sotomayor Torres, P. Gómez-Romero, J. Martorell, C. Ros, Controlling the electrochemical hydrogen generation and storage in graphene oxide by in-situ Raman spectroscopy, Carbon 200 (2022) 227–235, http://dx.doi.org/10.1016/j.carbon.2022.08.055.

[6] M.G. Betti, E. Placidi, C. Izzo, E. Blundo, A. Polimeni, M. Sbroscia, J. Avila, P. Dudin, K. Hu, Y. Ito, D. Prezzi, M. Bonacci, E. Molinari, C. Mariani, Gap opening in double-sided highly hydrogenated free-standing graphene, Nano Lett. 22 (7) (2022) 2971–2977, http://dx.doi.org/10.1021/acs.nanolett.2c00162.

[7] S. Casolo, O.M. Løvvik, R. Martinazzo, G.F. Tantardini, Understanding adsorption of hydrogen atoms on graphene, J. Chem. Phys. 130 (5) (2009) 054704, http://dx.doi.org/10.1063/1.3072333.

[8] C.-F. Cheng, J. Hussels, M. Niu, H.L. Bethlem, K.S.E. Eikema, E.J. Salumbides, W. Ubachs, M. Beyer, N. Hölsch, J.A. Agner, F. Merkt, L.-G. Tao, S.-M. Hu, C. Jungen, Dissociation energy of the hydrogen molecule at 10^{-9} accuracy, Phys. Rev. Lett. 121 (2018) 013001, http://dx.doi.org/10.1103/PhysRevLett.121.013001.

[9] H. Tachikawa, Hydrogen atom addition to the surface of graphene nanoflakes: A density functional theory study, Appl. Surf. Sci. 396 (2017) 1335–1342, http://dx.doi.org/10.1016/j.apsusc.2016.11.158.

[10] Y.S. Nechaev, T.N. Veziroglu, Thermodynamic aspects of the graphene/graphane/hydrogen systems: Relevance to the hydrogen on-board storage problem, Adv. Mater. Phys. Chem. 3 (2013) 255–280, http://dx.doi.org/10.4236/ampc.2013.35037.

[11] A. Rossi, S. Piccinin, V. Pellegrini, S. de Gironcoli, V. Tozzini, Nano-scale corrugations in graphene: A density functional theory study of structure, electronic properties and hydrogenation, J. Phys. Chem. C 119 (14) (2015) 7900–7910, http://dx.doi.org/10.1021/jp511409b.

[12] J.O. Sofo, A.S. Chaudhari, G.D. Barber, Graphane: A two-dimensional hydrocarbon, Phys. Rev. B 75 (2007) 153401, http://dx.doi.org/10.1103/PhysRevB.75.153401.

[13] V. Tozzini, V. Pellegrini, Reversible hydrogen storage by controlled buckling of graphene layers, J. Phys. Chem. C 115 (51) (2011) 25523–25528, http://dx.doi.org/10.1021/jp208262r.

[14] S. Goler, C. Coletti, V. Tozzini, V. Piazza, T. Mashoff, F. Beltram, V. Pellegrini, S. Heun, Influence of graphene curvature on hydrogen adsorption: Toward hydrogen storage devices, J. Phys. Chem. C 117 (22) (2013) 11506–11513, http://dx.doi.org/10.1021/jp4017536.

[15] K. Takahashi, S. Isobe, K. Omori, T. Mashoff, D. Convertino, V. Miseikis, C. Coletti, V. Tozzini, S. Heun, Revealing the multibonding state between hydrogen and graphene-supported Ti clusters, J. Phys. Chem. C 120 (24) (2016) 12974–12979, http://dx.doi.org/10.1021/acs.jpcc.6b05207.

[16] V.D. Camiola, R. Farchioni, T. Cavallucci, A. Rossi, V. Pellegrini, V. Tozzini, Hydrogen storage in rippled graphene: Perspectives from multi-scale simulations, Front. Mater. 2 (2015) http://dx.doi.org/10.3389/fmats.2015.00003.

[17] L. Basta, F. Bianco, A. Moscardini, F. Fabbri, L. Bellucci, V. Tozzini, S. Heun, S. Veronesi, Deterministic organic functionalization of monolayer graphene via high resolution surface engineering, J. Mater. Chem. C 11 (2023) 2630–2639, http://dx.doi.org/10.1039/D2TC04168E.

[18] L. Basta, A. Moscardini, F. Fabbri, L. Bellucci, V. Tozzini, S. Rubini, A. Griesi, M. Gemmi, S. Heun, S. Veronesi, Covalent organic functionalization of graphene nanosheets and reduced graphene oxide via 1, 3-dipolar cycloaddition of azomethine ylide, Nanoscale Adv. 3 (2021) 5841–5852, http://dx.doi.org/10.1039/D1NA00335F.

[19] F. Späth, W. Zhao, C. Gleichweit, K. Gotterbarm, U. Bauer, O. Höfert, H.-P. Steinrück, C. Papp, Hydrogenation and dehydrogenation of nitrogen-doped graphene investigated by X-ray photoelectron spectroscopy, Surf. Sci. 634 (2015) 89–94, http://dx.doi.org/10.1016/j.susc.2014.11.009, Graphene and Graphene Related Materials Growth on Surfaces.

[20] Y.S. Nechaev, N.M. Alexandrova, N.A. Shurygina, A.O. Cheretaeva, A.A. Pisarev, On the kinetic analysis of the hydrogen thermal desorption spectra for graphite and advanced carbon nanomaterials, Fullerenes Nanotubes Carbon Nanostruct. 28 (2) (2020) 147–149, http://dx.doi.org/10.1080/1536383X.2019.1680982.

[21] Y.-H. Hu, H.-L. Wan, K.-R. Tsai, C.-T. Au, Computer simulation of derivative TPD, Thermochim. Acta 274 (1996) 289–301, http://dx.doi.org/10.1016/0040-6031(95)02709-2.

[22] Y.S. Nechaev, N.M. Alexandrova, N.A. Shurygina, A.O. Cheretaeva, E.A. Denisov, E.K. Kostikova, Studying the states of hydrogen in Graphene, Graphite, and Steels, Bull. Russian Acad. Sci. 85 (2021) 701–708, http://dx.doi.org/10.3103/S1062873821070169.

[23] T.P. Senftle, S. Hong, M.M. Islam, S.B. Kylasa, Y. Zheng, Y.K. Shin, C. Junkermeier, R. Engel-Herbert, M.J. Janik, H.M. Aktulga, T. Verstraelan, A. Grama, A.C.T. van Duin, The ReaxFF reactive force-field: development, applications and future directions, npj Comput. Mater. 2 (1) (2016) 1–14.

[24] M. Kowalik, C. Ashraf, B. Damirchi, D. Akbarian, S. Rajabpour, A.C.T. van Duin, Atomistic scale analysis of the carbonization process for C/H/O/N-based polymers with the ReaxFF reactive force field, J. Phys. Chem. B 123 (25) (2019) 5357–5367, http://dx.doi.org/10.1021/acs.jpcb.9b04298.

[25] A.C.T. van Duin, S. Dasgupta, F. Lorant, W.A. Goddard, Reaxff: A reactive force field for hydrocarbons, J. Phys. Chem. A 105 (41) (2001) 9396–9409, http://dx.doi.org/10.1021/jp004368u.

[26] J.P. Perdew, K. Burke, M. Ernzerhof, Generalized gradient approximation made simple, Phys. Rev. Lett. 77 (1996) 3865–3868, http://dx.doi.org/10.1103/PhysRevLett.77.3865.

[27] S. Grimme, J. Antony, S. Ehrlich, H. Krieg, A consistent and accurate ab initio parametrization of density functional dispersion correction (DFT-D) for the 94 elements H-Pu, J. Chem. Phys. 132 (15) (2010) 154104.

[28] Y. Murata, T. Cavallucci, V. Tozzini, N. Pavliček, L. Gross, G. Meyer, M. Takamura, H. Hibino, F. Beltram, S. Heun, Atomic and electronic structure of si dangling bonds in quasi-free-standing monolayer graphene, Nano Res. 11 (2018) 864–873, http://dx.doi.org/10.1007/s12274-017-1697-x.

[29] T. Cavallucci, Y. Murata, M. Takamura, H. Hibino, S. Heun, V. Tozzini, Unraveling localized states in quasi free standing monolayer graphene by means of density functional theory, Carbon 130 (2018) 466–474, http://dx.doi.org/10.1016/j.carbon.2018.01.027.

[30] P. Giannozzi, O. Baseggio, P. Bonfà, D. Brunato, R. Car, I. Carnimeo, C. Cavazzoni, S. de Gironcoli, P. Delugas, F. Ferrari Ruffino, A. Ferretti, N. Marzari, I. Timrov, A. Urru, S. Baroni, Quantum ESPRESSO toward the exascale, J. Chem. Phys. 152 (15) (2020) 154105, http://dx.doi.org/10.1063/5.0005082.

[31] A.P. Thompson, H.M. Aktulga, R. Berger, D.S. Bolintineanu, W.M. Brown, P.S. Crozier, P.J. in 't Veld, A. Kohlmeyer, S.G. Moore, T.D. Nguyen, R. Shan, M.J. Stevens, J. Tranchida, C. Trott, S.J. Plimpton, LAMMPS - a flexible simulation tool for particle-based materials modeling at the atomic, meso, and continuum scales, Comp. Phys. Commun. 271 (2022) 108171, http://dx.doi.org/10.1016/j.cpc.2021.108171.

[32] A. Vashisth, M. Kowalik, J.C. Gerringer, C. Ashraf, A.C.T. van Duin, M.J. Green, ReaxFF simulations of laser-induced graphene (LIG) formation for multifunctional polymer nanocomposites, ACS Appl. Nano Mater. 3 (2) (2020) 1881–1890, http://dx.doi.org/10.1021/acsanm.9b02524.

[33] Z.G. Fthenakis, I.D. Petsalakis, V. Tozzini, N.N. Lathiotakis, Evaluating the performance of ReaxFF potentials for sp2 carbon systems (graphene, carbon nanotubes, fullerenes) and a new ReaxFF potential, Front. Chem. 10 (2022) http://dx.doi.org/10.3389/fchem.2022.951261.

[34] N. Melchioni, L. Bellucci, A. Tredicucci, F. Bianco, Operability timescale of defect-engineered graphene, Surf. Interfaces 37 (2023) 102662, http://dx.doi.org/10.1016/j.surfin.2023.102662.

[35] K.E. Whitener Jr., Review Article: Hydrogenated graphene: A user's guide, J. Vac. Sci. Tech. A 36 (5) (2018) 05G401, http://dx.doi.org/10.1116/1.5034433.

[36] M. Allen, D. Tildesley, Computer Simulation of Liquids, Oxford University Press, 2017, URL https://books.google.it/books?id=nlExDwAAQBAJ.

[37] G. Bussi, D. Donadio, M. Parrinello, Canonical sampling through velocity rescaling, J. Chem. Phys. 126 (1) (2007) 014101, http://dx.doi.org/10.1063/1.2408420.

[38] Z. Yang, Y. Sun, L.B. Alemany, T.N. Narayanan, W.E. Billups, Birch reduction of graphite. Edge and interior functionalization by hydrogen, J. Am. Chem. Soc. 134 (45) (2012) 18689–18694, http://dx.doi.org/10.1021/ja3073116.

[39] R.A. Schäfer, J.M. Englert, P. Wehrfritz, W. Bauer, F. Hauke, T. Seyller, A. Hirsch, On the way to graphane—Pronounced fluorescence of polyhydrogenated graphene, Angew. Chemie Int. Ed. 52 (2) (2013) 754–757, http://dx.doi.org/10.1002/anie.201206799.

[40] S. Claramunt, A. Varea, D. López-Díaz, M.M. Velázquez, A. Cornet, A. Cirera, The importance of interbands on the interpretation of the Raman spectrum of graphene oxide, J. Phys. Chem. C 119 (18) (2015) 10123–10129, http://dx.doi.org/10.1021/acs.jpcc.5b01590.

Multi-methodological analysis of hydrogen desorption from graphene

Francesco Delfino[a], Carles Ros[b], Sidney M. Palardonio[b], Nina M. Carretero[c], Sebastián Murcia-López[c], Juan Ramón Morante[c], Jordi Martorell[b,d], Zacharias G. Fthenakis[a], Mauro Francesco Sgroi[e,1], Valentina Tozzini[a,f], Luca Bellucci[a,*]

[a]*Istituto Nanoscienze del Consiglio Nazionale delle Ricerche (CNR-NANO), NEST-SNS, Piazza San Silvestro, 12, Pisa, 56127, Italy*
[b]*ICFO, Institut de Ciencies Fotoniques, The Barcelona Institute of Science and Technology, Castelldefels, Spain*
[c]*IREC, Fundacion Instituto de Investigacion de la Energía de Cataluña, Jardins de les Dones de Negre 1, 2ª pl., Sant' Adrià del Besòs, Barcelona, 08930, Spain*
[d]*UPC, Departament de Física, Universitat Politecnica de Catalunya, , Terrassa, 08222, Spain*
[e]*Department of Chemistry and NIS, University of Turin, Via Pietro Giuria 7, Torino, 10125, Italy*
[f]*INFN Sezione di Pisa, Largo Bruno Pontecorvo, Pisa, 56127, Italy*

Supporting Information

S1. Hydrogenated model systems details

The six model systems that were used to apply the simulated TPD procedure (S1). On average, the models exhibit a coverage of 63%. The hydrogen distribution is random in cis or trans conformations (Fig. S2). Additionally, Models 2, 3, 5, and 6 display small defects where sp^2 carbon atoms at the edges are hydrogenated (Fig.S2).

*luca.bellucci@nano.cnr.it

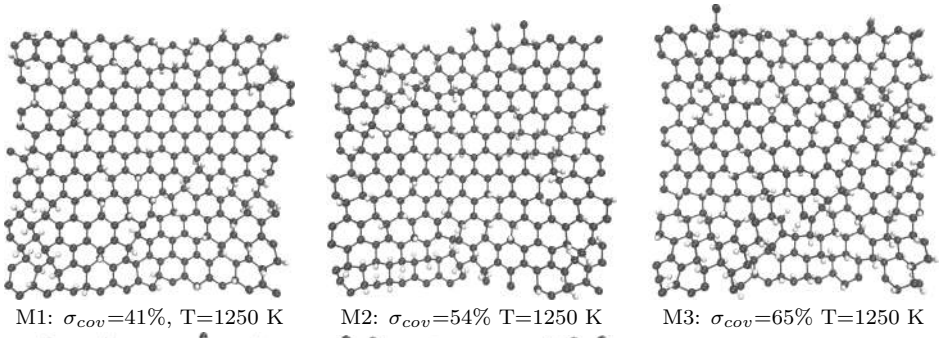

Figure S1: The six initial hydrogenated models (Ms) are presented at various specified coverages (σ_{cov}), expressed as the ratio of the number of H to the total number of C in percentage. The temperature (T) of the H reservoir to which the systems are exposed is also indicated.

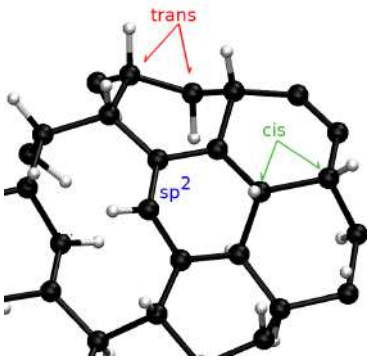

Figure S2: Examples of cis (green) and trans (red) hydrogen conformations are shown. In blue, a sp^2 hydrogenated carbon atom positioned at the edge of a defect is highlighted.

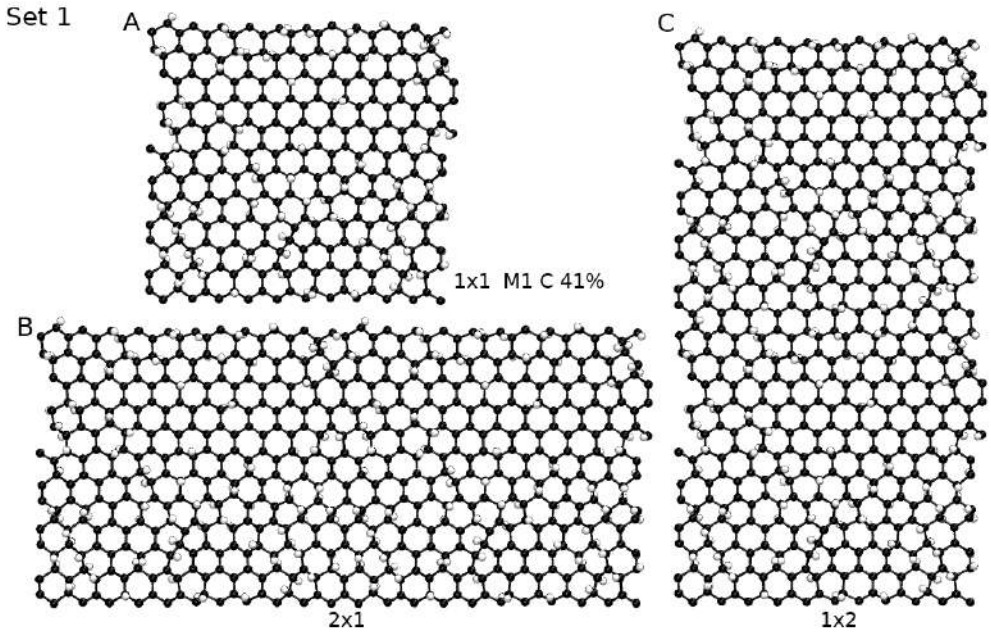

Figure S3: Example of a set of systems at fixed coverage originates from the original M1 model (A) with a H coverage of 41% (see Fig. S1) and used to evaluate averaged TPD reported in Figure S6 and Figure S7. B) Replica along the x-axis. C) Replica along the y-axis.

S2. Experimental XRD experiments

XRD diffractograms show that the interplanar spacing increases due to hydrogen bound to the surface of graphene layers, with the peak (002) at 2θ = 18.90° for the pristine layer and 2θ = 26.18° for the hydrogenated layer, respectively, in accordance with other similar works[1].

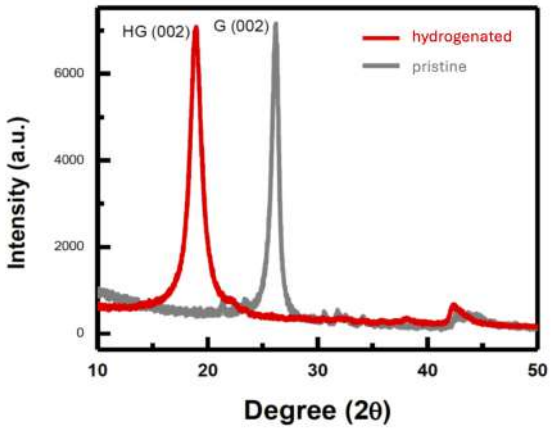

Figure S4: The XRD diffractogram of both hydrogenated and non-hydrogenated samples, supplied by Xlynx Materials Inc..

S3. Experimental TPD spectra

TPD experiments are illustrated in Figure S5. The thermal conductivity detector (TCD) signal (black line upper plots) shows the conductivity change from all gases emitted simultaneously, meanwhile, the mass spectrum (MS) shows the individual desorption of every species. It can be seen that water molecules are desorbed starting at 340 K (67 °C) and have a significant impact on the TCD detection. Meanwhile, hydrogen molecules start desorbing at 425 K (152 °C) but with a smaller impact in the conductivity detector, caused by its way smaller mass. There are two extra H_2O peaks in the 500-600 K region, which could be generated by the presence of -O- and -OH functional groups impurities. Also, small traces of ammonia and its ionized species are detected.

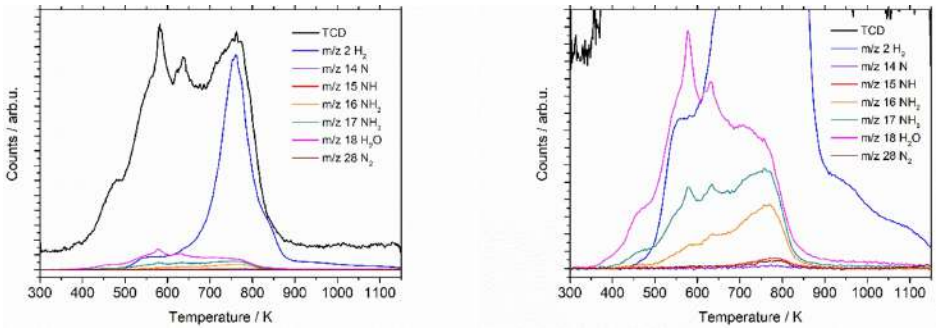

Figure S5: Upper plots: TPD raw spectra of highly hydrogenated samples of Fig. 2 (a). The signal of TCD (black line) is indicative of all desorbed products simultaneously, which can be separated by the mass spectrometer (MS, colored lines). On the right, same experiment but zoomed in to show better the low signal parts.

S4. Simulated TPD profiles

Figure S6 and Figure S7 report the TPD spectra for the six desorption simulation set (Fig. S3) at different starting coverages (Fig. S1) for the two β values.

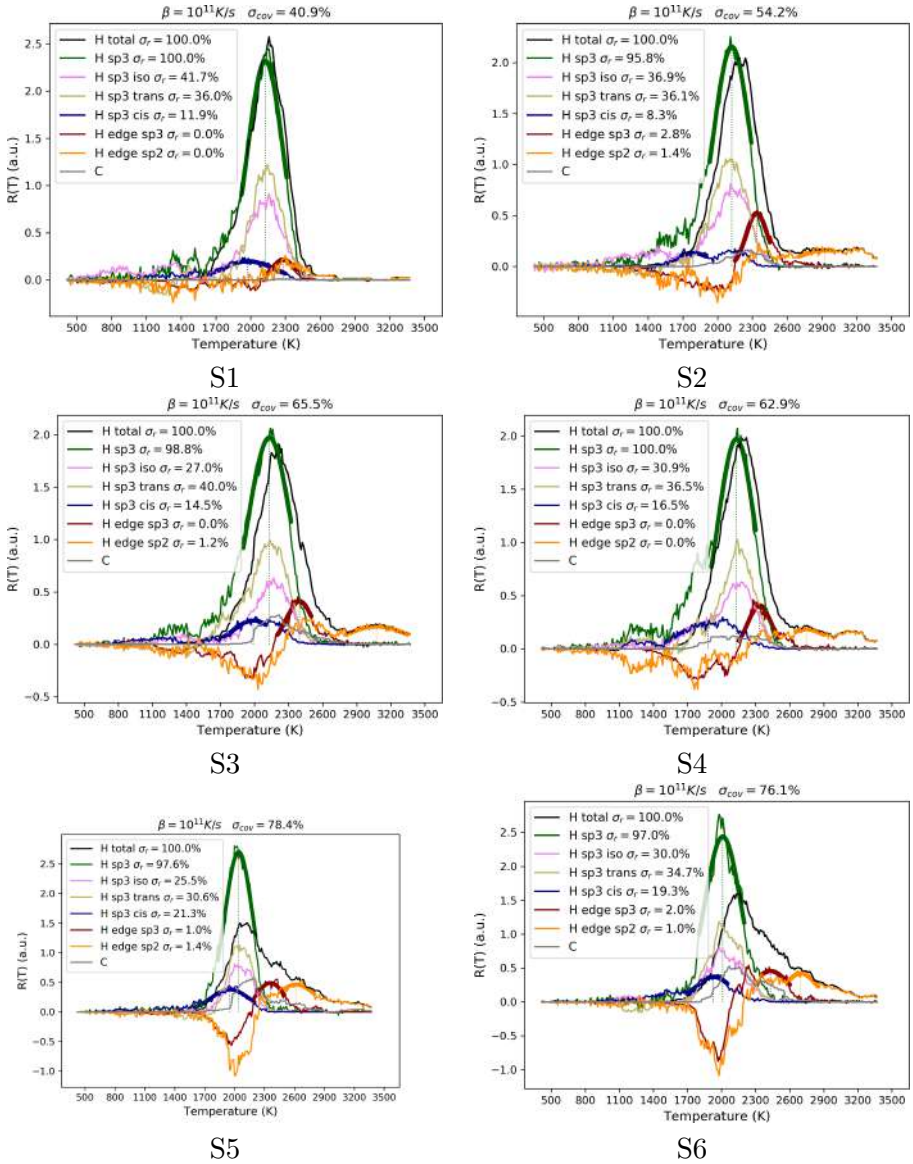

Figure S6: TPP spectra for the set S1-6 for $\beta = 10^{11}$.

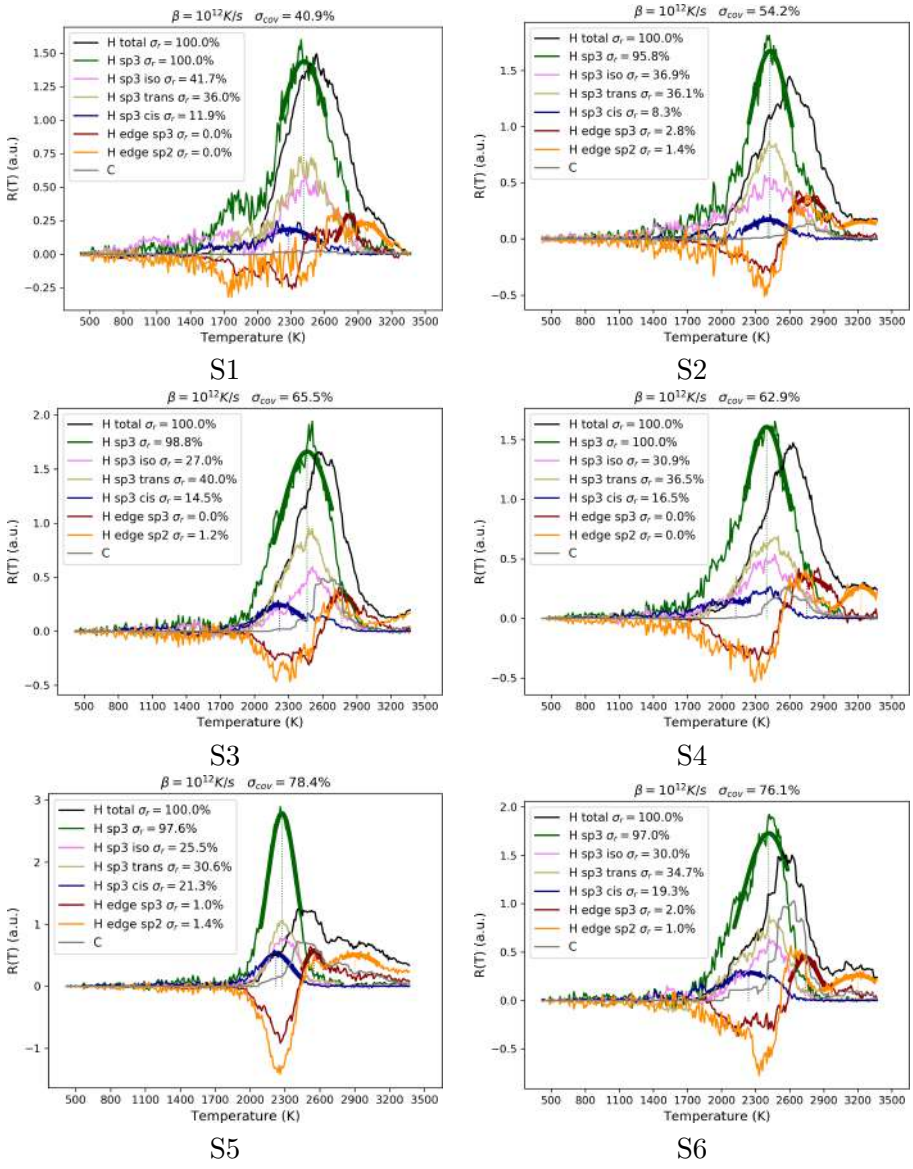

Figure S7: TPD spectra for the set S1-6 for $\beta = 10^{12}$.

S5. Energy barriers direct calculations, details

Figs. S8 reports the results of direct calculations of the desorption energy profiles with ReaxFF, as per the visual legend.

Fig. S9 reports a summary plot of the E_d values extracted from TPD fits as a function of the starting coverage of the sheet. Colors coding in the visual legend and the caption.

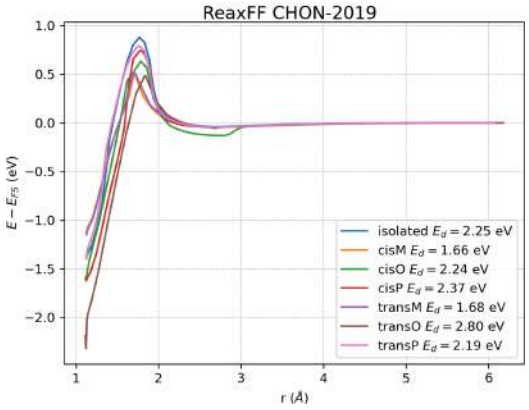

Figure S8: Desorption energy profiles obtained with the neb method and the ReaxFF for different ideal hydrogen configurations.

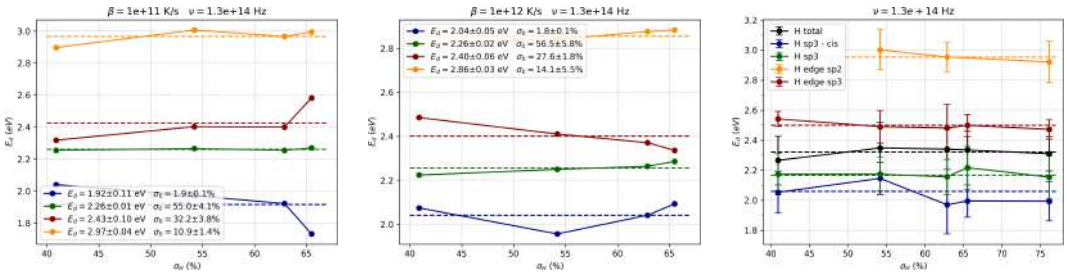

Figure S9: (a, b, c) Energy barriers of different desorption processes as a function of the initial hydrogen coverage. Color code: black, sum of all processes; blue, sp^3 cis; green, sum of all sp^3 in the bulk; yellow, sp^2 on the edges; red, sp^3 on the edges. In (a , b) energy barriers are calculated with the convolution fit method, respectively for $\beta = 10^{11} K/s$ and $\beta = 10^{12} K/s$. Average values are given in the visual legend, and also reported in Table 1. In (c) energy barriers are calculated with the regression fit method.

Fig. S10 reports a summary of the DFT calculations for sample cases. Two different conformations of the isolated H are shown, with different starting corrugation, displaying different E_d values (reported in the caption). The three cases where the bound state is observed weakly magnetic are also shown, with the sheet colored according to magnetization, as explained in the caption.

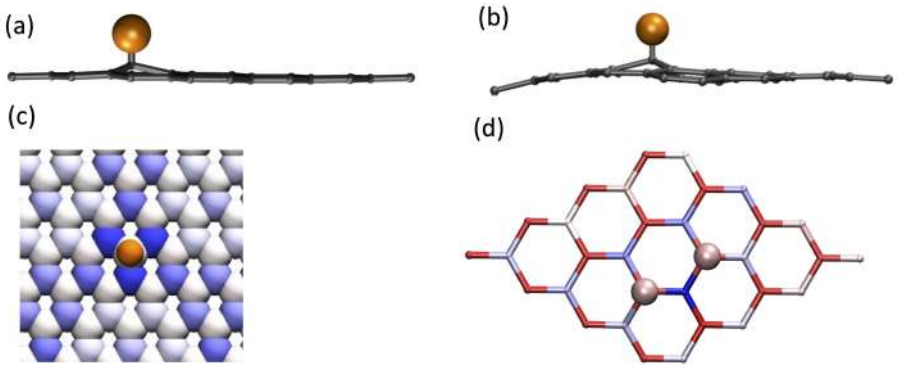

Figure S10: Sample structures from DFT calculations. (a) and (b): isolated H structures, in the completely flat sheet and in the weakly corrugated one, respectively. The E_d values for the H desorption from these conformations are 0.97eV and 1.64eV respectively. (c) Top view of (a), with the sheet represented as vdW-filled balls colored according to magnetization, blue representing magnetized sites. The total value of the M_z is 1 Bohr magnetons. (d) the same for the cis-meta dimer, with the bond network of graphene represented by sticks. In this case, the color shading is such that the neutral sites appear reddish, and the polarized one in blue. The same alternating structure of polarized/unpolarized sites of the two inequivalent sublattices is observed as in the previous case, enhanced by the fact that in this case two carbons of the same sublattice are occupied by the H. The total value of magnetization is 2 in this case. The case trans-meta (not reported) brings a very similar magnetization distribution.

Table S1 reports a summary of the previous literature values of binding and barrier energies.

System	E_b^{at}	E_b^{mol}	E_a^{at}	E_d^{at}	E_a^{mol}	E_d^{mol}	cover	year	ref
graphane chair	−6.56	*−4.33*					100%	2007	[2]
graphane boat	−6.50	*−4.27*					100%		[2]
graphane	−2.5	*−0.3*					100%	2013	[3]
isolated	−1.44	*0.8*					0	2008	[4]
dim ortho cis	−0.909	*1.32*							[4]
dim ort trans	−0.504	*1.726*							[4]
dim para cis	−1.406	*0.824*							[4]
isolated	−0.84	*1.39*	0.20	1.04			0	2009	[5]
2nd ortho	−1.934	*1.30*							[5]
2nd meta	−0.802	*1.42*							[5]
2nd para	−1.894	*0.336*							[5]
curved sheet	−[2.5,0]	*[-0.27,+2.3]*			[0.7-2.5]	[0,1.5]		2011	[6]
clusters one side	−[1.9,1.0]	*[0.33,1.23]*					0-40%	2015	[7]
isolated	−[0.64,1.23]	*[1.59,1.00]*	[0.22,0.30]	[0.86,1.53]				2017	[8]

Table S1: Binding and barrier energies as defined in Fig. 1 from literature expressed in eV. Energies are per H atom. E_b^{at} and E_b^{mol} are both binding energies per atom, but referred to the atomic or molecular hydrogen. The value in Roman font is extracted from the papers, the one in *italics* calculated with the formula $E_b^{mol} - E_b^{at} = 2.23$ eV. The two values of ref [2] are for graphane in armchair and boat configurations. The coverage in the case of dimers is left undefined: dimers are more likely at high coverage, but even at low coverage the dimers conformation is favored over the isolated one.

References

[1] Z. Yang, Y. Sun, L. B. Alemany, T. N. Narayanan, W. E. Billups, Birch reduction of graphite. edge and interior functionalization by hydrogen, J Am Chem Soc 134 (45) (2012) 18689–18694. doi:10.1021/ja3073116.

[2] J. O. Sofo, A. S. Chaudhari, G. D. Barber, Graphane: A two-dimensional hydrocarbon, Phys. Rev. B 75 (2007) 153401. doi:10.1103/PhysRevB.75.153401.

[3] Y. S. Nechaev, T. N. Veziroglu, Thermodynamic aspects of the graphene/graphane/hydrogen systems: Relevance to the hydrogen on-board storage problem, Adv. Mater. Phys. Chem. 3 (2013) 255–280. doi:10.4236/ampc.2013.35037.

[4] D. W. Boukhvalov, M. I. Katsnelson, A. I. Lichtenstein, Hydrogen on graphene: Electronic structure, total energy, structural distortions and magnetism from first-principles calculations, Phys. Rev. B 77 (2008) 035427. doi:10.1103/PhysRevB.77.035427.

[5] S. Casolo, O. M. Løvvik, R. Martinazzo, G. F. Tantardini, Understanding adsorption of hydrogen atoms on graphene, J. Chem. Phys. 130 (5) (2009) 054704. doi:10.1063/1.3072333.

[6] V. Tozzini, V. Pellegrini, Reversible hydrogen storage by controlled buckling of graphene layers, J. Phys. Chem. C 115 (51) (2011) 25523–25528. doi:10.1021/jp208262r.

[7] A. Rossi, S. Piccinin, V. Pellegrini, S. de Gironcoli, V. Tozzini, Nano-scale corrugations in graphene: A density functional theory study of structure, electronic properties and hydrogenation, J. Phys. Chem. C 119 (14) (2015) 7900–7910. doi:10.1021/jp511409b.

[8] H. Tachikawa, Hydrogen atom addition to the surface of graphene nanoflakes: A density functional theory study, Appl. Surf. Sci. 396 (2017) 1335–1342. doi:10.1016/j.apsusc.2016.11.158.